International Journal of Fracture **119:** 145–159, 2003.

Asymptotic Stress Intensity Factor Density Profiles for Smeared-Tip Method for Cohesive Fracture

ZDENĚK P. BAŽANT and GOANGSEUP ZI
Department of Civil and Environmental Engineering, Northwestern University, Evanston, Illinois 60208, U.S.A.

Received 19 December 2001; accepted in revised form 26 August 2002

Abstract. The paper presents a computational approach and numerical data which facilitate the use of the smeared-tip method for cohesive fracture in large enough structures. In the recently developed K-version of the smeared tip method, the large-size asymptotic profile of the stress intensity factor density along a cohesive crack is considered as a material characteristic, which is uniquely related to the softening stress-displacement law of the cohesive crack. After reviewing the K-version, an accurate and efficient numerical algorithm for the computation of this asymptotic profile is presented. The algorithm is based on solving a singular Abel's integral equation. The profiles corresponding to various typical softening stress-displacement laws of the cohesive crack model are computed, tabulated and plotted. The profiles for a certain range of other typical softening laws can be approximately obtained by interpolation from the tables. Knowing the profile, one can obtain with the smeared-tip method an analytical expression for the large-size solution to fracture problems, including the first two asymptotic terms of the size effect law. Consequently, numerical solutions of the integral equations of the cohesive crack model as well as finite element simulations of the cohesive crack are made superfluous. However, when the fracture process zone is attached to a notch or to the body surface and the cohesive zone ends with a stress jump, the solution is expected to be accurate only for large-enough structures.

Key words: Fracture, size effect, scaling, cohesive crack, quasibrittle materials, asymptotic approximation, smeared-tip method, computation.

1. Introduction

The cohesive crack model has become generally accepted as a realistic simplification of quasi-brittle fracture of materials such as concrete, rock, sea ice, toughened ceramics, and various composites. In this model, all of the inelastic deformation is lumped into a line, which makes it possible to treat the whole body as elastic. The basic idea of the cohesive crack model, originated by Barenblatt (1959; 1962), is that the stress sigularity at the crack tip is eliminated by the cohesive stress acting on the crack surfaces. The cohesive (or fictitious) crack model has been refined, formulated numerically, and adapted to various materials by a number of researchers (Palmer and Rice, 1973; Knauss, 1973, 1974; Hillerborg et al., 1976; Kfouri and Rice, 1977; Petersson, 1981; Needleman, 1990; Planas and Elices, 1992, 1993; Planas et al., 1994; Bažant and Li, 1995; Smith, 1999; Zi and Bažant, 2002). For a detailed exposition, see, e.g., Bažant and Planas (1998).

An effective approach to solutions with the cohesive crack model is the smeared-tip method, in which the solution is represented as a superposition of infinitely many solutions for sharp cracks of various crack lengths and infinitely small stress intensity factors. The tips of these cracks are continuously distributed (i.e., smeared) along the cohesive crack (Planas and Elices, 1986, 1992, 1993; Bažant, 1990; Bažant and Beissel, 1994; Bažant and Planas, 1998). In this manner, the solution for a structure with a cohesive crack, under a given load, may be con-

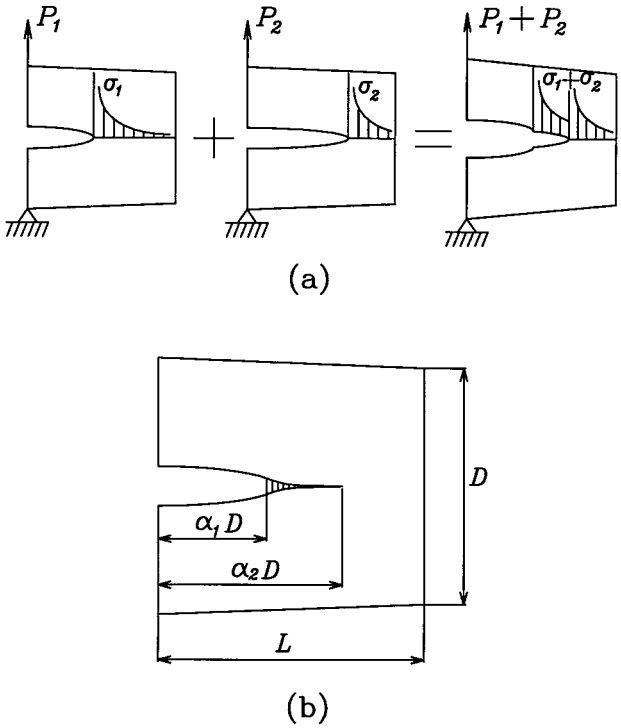

Figure 1. (a) Superposition of LEFM cracks and (b) notations of the cohesive crack model

structed according to the linear elastic fracture mechanics (LEFM) if it is known how the stress intensity factor K_I and the crack opening profile for a unit load depends on the crack tip location. For large enough structures, the asymptotic near-tip crack opening profile corresponding to the stress intensity factor may be used as an approximation and then it suffices to know K_I as a function of the relative crack length α. The smeared-tip approach is computationally more efficient and better suited for obtaining analytical asymptotic approximations than the compliance function approach used by Hillerborg et al. (1976), Petersson (1981) and others (Needleman, 1990).

Once the asymptotic stress intensity factor density, called the q-profile, corresponding to a given stress-separation law of the cohesive crack model is established, it can be used for simple asymptotic solutions for a structure of any geometry for which the stress intensity factor as a function of α is known. The objective of this paper is to present solutions of the q-profile for various typical stress-separation laws used for quasibrittle materials. The K-version of the smeared tip method and the size effect laws derived from it, which were outlined by Bažant (2001) and derived in detail by Bažant (2002), will be reviewed to introduce the subject.

2. Review of K-Version of Smeared-Tip Method

In the smeared-tip method, one superposes the LEFM solutions of the given structure for various lengths of sharp cracks (Figure 1a), whose tips are continuously distributed (smeared) along the assumed crack path. Such superposition is used to represent the solution for a cohesive crack (Figure 1b). Any opening profiles and any stress profiles can be represented in this way.

For a single LEFM mode I crack,

$$P = b\sqrt{D}\,K_I(\alpha)/k(\alpha) \qquad (\alpha = a/D) \tag{1}$$

where P = applied load or a parameter of a system of distributed or concentrated loads, b = body thickness, K_I = mode I stress intensity factor (SIF) for a crack tip located at α; $k(\alpha) = \sqrt{g(\alpha)}$ = dimensionless SIF function (i.e., K_I for $D = b = P = 1$). For a body of given geometry, $\alpha = a/D$ = relative crack length, $g(\alpha)$ = dimensionless energy release rate function; a = actual crack length, and D = characteristic size (or dimension) of the structure. The stress σ on the crack line ahead of the crack tip and the crack opening width w behind the crack tip are, according to LEFM,

$$\sigma(\xi) = K_I(\alpha)S(\xi,\alpha), \qquad \alpha \in (0,\xi) \tag{2}$$

$$S(\xi,\alpha) = \frac{1}{\sqrt{2\pi D(\xi-\alpha)}}[1+\ b_1(\xi,\alpha)(\xi-\alpha) + b_2(\xi,\alpha)(\xi-\alpha)^2 + \dots] \tag{3}$$

$$w(\xi) = K_I(\alpha)\,W(\xi,\alpha), \qquad \alpha \in (\xi, L/D) \tag{4}$$

$$W(\xi,\alpha) = \frac{\sqrt{32}}{E'\sqrt{\pi}}\sqrt{D(\alpha-\xi)}\ [1 + c_1(\xi,\alpha)(\alpha-\xi) + c_2(\xi,\alpha)(\alpha-\xi)^2 + \dots] \tag{5}$$

where $E' = E/(1-\nu^2)$ for plane stress, $E' = E$ for plane strain, E = Young's modulus, ν = Poisson ratio, L = length of assumed crack propagation path, $\xi = x/D$ = dimensionless coordinate along the crack path; σ = cohesive (crack bridging) stress, w = crack opening width (= separation of crack faces), $b_1, b_2, \dots, c_1, c_2, \dots$ are nonsingular dimensionless functions of ξ and α which depend on the geometry (shape) of the structure. Functions $b_1, b_2, \dots, c_1, c_2, \dots$ can be approximated by polynomials obtained by curve-fitting finite element results.

The applied load P, cohesive stress σ and crack opening width w obtained by superposition of (1), (2) and (4) for infinitely many cracks with continuously distributed (smeared) tips may in general be written as

$$P = \int dP = b\sqrt{D}\int_0^{L/D} \frac{\mathrm{d}K_I(\alpha)}{k(\alpha)} \tag{6}$$

$$\sigma(\xi) = \int_0^{\xi} S(\xi,\alpha)\,\mathrm{d}K_I(\alpha), \quad w(\xi) = \int_{\xi}^{L/D} W(\xi,\alpha)\,\mathrm{d}K_I(\alpha) \tag{7}$$

where L is the final length of the crack at total break and $\mathrm{d}K_I(\alpha)$ is the SIF of the smeared tips lying between α and $\alpha + \mathrm{d}\alpha$. The relative coordinates at the beginning and the end of the cohesive portion of the crack, representing the fracture process zone (FPZ), will be labeled as α_1 and α_2 (Figure 1b). It will be convenient to introduce a further dimensionless coordinate

$$\rho = \frac{\alpha-\alpha_1}{2\theta}, \quad \text{with} \quad \theta = \frac{l_f}{D} = \tfrac{1}{2}(\alpha_2-\alpha_1) \tag{8}$$

where α_1 = the end of the stress-free crack portion, α_2 = the tip of the cohesive crack (end of FPZ), and l_f = one half of FPZ length.

The q-profile along the FPZ may be characterized as

$$\mathrm{d}K_I(\alpha) = \frac{K_c D}{2l_f} q[\rho(\alpha)]\,\mathrm{d}\alpha = K_c\, q(\rho)\,\mathrm{d}\rho \tag{9}$$

where K_c = fracture toughness (critical SIF), $q(\rho)$ = q-profile = dimensionless SIF density as a function of dimensionless crack length ρ. It is assumed that function $q(\rho)$ is such that the function $q(\rho)/\sqrt{|\omega - \rho|}$ be integrable for $0 < \omega < 1$; see Equations (3) and (7). This also guarantees the total SIF at the cohesive crack tip to vanish (note that boundedness of $q(\rho)$ is sufficient but not necessary to satisfy these conditions). For $D \to \infty$ the fracture process zone in the relative coordinate α becomes a point, and so LEFM must apply, which means that $\int \mathrm{d}K_I = K_c$ = fracture toughness of the material, or

$$I_1 = \int_0^1 q(\rho)\mathrm{d}\rho = 1 \tag{10}$$

The smeared-tip method can be formulated in two versions. In the original version, labeled here the P-version (Planas and Elices, 1986; 1992, 1993; Bažant, 1990; Bažant and Beissel, 1994; Bažant and Planas, 1998), the SIF of the smeared crack tips between α and $\alpha + d\alpha$ was associated not with an SIF increment $dK_I(\alpha)$ but with a load contribution $dP = p(\alpha)Dd\alpha$ where $p(\alpha)$ was the load-sharing distribution. The present approach is labeled the K-version since the smeared crack tips are associated with the increments of K_I. The relation between $p(\alpha)$ in P-version and $q(\alpha)$ in K-version is

$$p(\alpha) = \frac{bK_c\sqrt{D}}{2l_f k(\alpha)} q[\rho(\alpha)] \tag{11}$$

Unlike the asymptotic q-profile $q(\rho)$, the asymptotic distribution $p(\alpha)$ is not size- and shape-independent, and so its asymptotic form is not a material property. Although Planas and Elices (1992, 1993) gave the expression for function $q(\rho)$, they used in their asymptotic analysis the P-version only. The difference between the P- and K-versions is of course nothing but a substitution of a new variable, but the K-version is much more convenient.

For sufficiently large structures, the higher order terms with functions $b_1, b_2, \ldots, c_1, c_2, \ldots$ may be neglected. Then Equations (7) and (8) simplify as follows:

$$\sigma(\rho) = \frac{K_c}{2\sqrt{\pi l_f}} S(\rho), \qquad S(\rho) = \int_0^\rho \frac{q(\omega)\mathrm{d}\omega}{\sqrt{\rho - \omega}} \tag{12}$$

$$w(\rho) = \frac{16K_c\sqrt{l_f}}{E'\sqrt{\pi}} W(\rho), \quad W(\rho) = \int_\rho^1 q(\omega)\sqrt{\omega - \rho}\mathrm{d}\omega \tag{13}$$

It will be convenient to write these equations also as

$$\sigma(\rho) = f_t \frac{S(\rho)}{S(1)}, \qquad w(\rho) = w_f \frac{W(\rho)}{W(0)} \tag{14}$$

where f_t = tensile strength of material and w_f = crack opening displacement at which the cohesive stress σ completely reduces to zero.

If K_c, l_f and the profile $q(\rho)$ are known, and if the structure is so large that the FPZ is fully developed (Smith, 1995, 1999), Equations (12) and (13) provide a parametric description of the stress-displacement curve $\sigma(w)$ of the cohesive crack model. Indeed, choosing a series of values of ρ, the corresponding pairs of w and σ can be obtained by evaluating the integrals $S(\rho)$ and $W(\rho)$, which are independent of structure size and shape. Thus, for each K-profile, there exists a corresponding stress-displacement curve (softening law) $\sigma(w)$ of the cohesive crack model. Vice versa, assuming this relationship to be invertible, one can find for each f_t and w_f the values of K_c, l_f and function $q(\rho)$. So the q-profile, $q(\rho)$, and the FPZ length, $2l_f$, are alternative material properties. A cohesive crack model defined by the *q-profile* is asymptotically equivalent to the standard cohesive crack model defined by the stress-displacement curve. For aymptotic analysis, a fixed q-profile can be used, along with l_f as the material fracture characteristic instead of the standard softening law.

If the shape of the softening law is fixed (i.e., if only vertical and horizontal scalings of a given softening curve are considered), as specified by RILEM Recommendation for concrete, the cohesive crack model is characterized by only two material parameters, which may be chosen either as f_t and w_f or as f_t and G_F where G_F = fracture energy = area under the complete curve of stress versus crack opening displacement. According to Irwin's relation,

$$G_F = K_c^2 \,/\, E' \tag{15}$$

To relate l_f to the basic parameters of the cohesive crack model, Rice's J-integral (Rice, 1968) giving the energy flux J into a fully developed FPZ may be utilized. The J-integral path must envelop the entire fracture process zone. Following Rice (1968), we choose a J-integral path that begins at the lower crack face at α_1, runs along this face to α_2, then along an infinitely small circle around the cohesive crack tip, and finally back to α_1 along the opposite crack face;

$$\begin{aligned} J &= \int_{\alpha_1}^{\alpha_2} \sigma(\alpha) \frac{\mathrm{d}[-w(\alpha)/2]}{\mathrm{d}\alpha}\mathrm{d}\alpha + \int_{\alpha_2}^{\alpha_1} \sigma(\alpha) \frac{\mathrm{d}[w(\alpha)/2]}{\mathrm{d}\alpha}\mathrm{d}\alpha \\ &= -\int_0^1 \sigma(\rho) \frac{\mathrm{d}w(\rho)}{\mathrm{d}\rho}\mathrm{d}\rho \end{aligned} \tag{16}$$

(which further yields Rice's relation $J = \int_0^{w_f} \sigma \,\mathrm{d}w$). If the FPZ is fully developed (i.e. if $\sigma = 0$ at $\rho = 0$), it can move forward only if $J = G_F$, and so this condition must be met asymptotically. Assuming this, substituting Equations (12) and (13) or (7), and taking into account Equation (15), one obtains

$$J = \frac{2I_0^2}{\pi} G_F = \frac{f_t w_f I_0^2}{2S(1)W(0)} \tag{17}$$

with the notation

$$I_0 = \sqrt{\int_0^1 \left(\int_0^\rho \frac{q(\omega)\,\mathrm{d}\omega}{\sqrt{\rho - \omega}} \right) \left(\int_\rho^1 \frac{q(\eta)\,\mathrm{d}\eta}{\sqrt{\eta - \rho}} \right) \mathrm{d}\rho} \tag{18}$$

Since $J = G_F$ asymptotically, it follows from (17) that

$$I_0 = \sqrt{\pi/2}, \qquad 4S(1)W(0)G_F = \pi f_t w_f \tag{19}$$

To determine the half-length l_f of the fracture process zone, one may now express from (12) the condition $\sigma(1) = f_t$. Thus, taking into account the last expressions in (17) and (19), one obtains

$$l_f = \frac{S^2(1)}{\pi} l_{ch} = \frac{\pi}{16\, W^2(0)} \frac{E' w_f^2}{G_F}, \quad l_{ch} = \frac{K_c^2}{4 f_t^2} \tag{20}$$

where l_{ch} represents Irwin's characteristic length. Now it should be noted that, in view of Equations (10) and (13), $W(0) \leq 1$, and so a lower bound on the half-length of the fracture process zone, for any shape of the stress-displacement law, is

$$l_{f\,\min} = \frac{\pi}{16} \frac{E' w_f^2}{G_F} \tag{21}$$

This lower bound was derived in a different way by Planas and Elices (1992, Equations 4.23 and 4.26).

The fact that neither D nor $k(\alpha)$ appears in (20) confirms that the hypothesis of size- and shape-independence of l_f agrees with the neglect of functions $b_1, b_2, \ldots, c_1, c_2, \ldots$ for large sizes. According to Equations (6) and (9), the nominal strength of the structure, which is a load parameter defined as $\sigma_N = P/bD$, may now be expressed as

$$\sigma_N = \frac{K_c}{\sqrt{D}} \int_0^1 \frac{q(\rho)\, \mathrm{d}\rho}{k[\alpha(\rho)]} \tag{22}$$

If the $q(\rho)$-profile along with l_f and $k(\alpha)$ are known, then σ_N can be evaluated from (22). In this manner, the large-size asymptotic size effect curve of the cohesive crack model can be computed for any given structure geometry provided that the function $k(\alpha)$ characterizing the geometry is known. For many geometries, this function is given in handbooks (Tada et al., 1985; Murakami, 1986), and for others it can be adequately approximated by curve-fitting elastic finite element results.

The size effects can be classified into three cases according to the geometry of the structure. In each case, the asymptotic size effect can be obtained from the asymptotic expansion of (22) in terms of the powers of θ, as suggested by Bažant (2001). Only the resulting size effect laws are listed below. The detailed derivations, including an appraisal of the role of various higher-order terms, are given by Bažant (2002). The first case is the case of positive geometry ($k'(\alpha) > 0$), where the fracture starts from the notch or a pre-existing stress-free (fatigued) crack. As expected, the analysis leads in this case to the classical size effect law proposed in Bažant (1983, 1984), i.e.

$$\sigma_N = \sigma_0 \left(1 + \frac{D}{D_0}\right)^{-1/2} \tag{23}$$

in which

$$\sigma_0 = \frac{K_c}{k_0 \sqrt{D_0}} \tag{24}$$

$$D_0 = \gamma_0 l_f = \frac{\gamma_0}{\pi} S^2(1) l_{ch} = \frac{4k_0'}{k_0} I_2 l_f = \frac{4k_0'}{\pi k_0} \frac{K_c^2}{f_t^2} I_2 S^2(1) \tag{25}$$

with the notations

$$\gamma_0 = \frac{4k_0'}{k_0} I_2, \qquad I_2 = \int_0^1 q(\rho)\, \rho\, \mathrm{d}\rho \tag{26}$$

Here k_0 = dimensionless stress intensity factor for $\alpha = \alpha_0$ = notch tip. A point to note from (25) is that the transitional size D_0 depends on the softening law. This means that the brittleness number of a structure, defined as $\beta = D/D_0$, depends on the material used.

Structures may also fail at the initiation of fracture from a smooth surface of the body or in the interior, which is case 2. A typical example is the standard test of the modulus of rupture of concrete beams. The size effect is written as

$$\sigma_N = \sigma_\infty \left(1 + \frac{D_b}{D}\right) \tag{27}$$

in which

$$\sigma_\infty = \frac{K_c I_3}{\sqrt{2g_0' l_f}}, \quad D_b = \frac{I_4\langle -g_0''\rangle}{2I_3 g_0'} l_f = \frac{I_4\langle -g_0''\rangle}{I_3 g_0'} \frac{1}{2\pi} S^2(1) l_{ch} \tag{28}$$

and

$$I_3 = \int_0^1 \frac{q(\rho)}{\sqrt{\rho}} d\rho, \qquad I_4 = \int_0^1 q(\rho)\sqrt{\rho}\, d\rho \tag{29}$$

(where $I_3 \geq 1$ and $I_4 \leq 1$). Here, g_0 = value of dimensionless energy release rate function for $\alpha = \alpha_0$ = notch tip. The Macauley brackets $\langle .. \rangle$ in (28) represents the positive part of the argument.

When the initial fracture geometry is negative, i.e., $k'(\alpha) < 0$, the crack grows stably under increasing load (an example is a panel with a small centric crack loaded on the crack faces). Failure under load control will occur only when the fracture geometry changes from negative to positive, which is case 3. The size effect then takes the form

$$\sigma_N = \sigma_0 \left(\frac{D_1}{D + D_1} + \frac{D}{D_0}\right)^{-1/2} \tag{30}$$

in which

$$D_1 = 4k_0 k_0'' I_5 \left(\frac{l_f \sigma_0}{K_c}\right)^2, \qquad D_0 = \left(\frac{K_c}{k_0 \sigma_0}\right)^2 \tag{31}$$

and, since $\rho_0 = \rho(\alpha_0) = \frac{1}{2}$

$$I_5 = \int_0^1 (\rho - \tfrac{1}{2})^2 q(\rho) d\rho \tag{32}$$

The difference between the optimum data fits with (23) and (30) is normally less than the scatter of test results.

The value of the small-size nominal strength σ_0 cannot be determined from the present asymptotic theory. It can be determined by using plastic analysis to solve the cohesive crack model for the case that $D \ll l_f$. In that case the cohesive stress along the entire crack path is nearly uniform, as if the crack were filled by a plastic glue, and the analysis proves that σ_0 must be finite.

3. Computation of *q*-Profiles

As mentioned before, the asymptotic q-profile has a one-to-one relationship to a softening law, and may therefore be regarded as a material property. If Equations (12) and (13) are substituted into the dimensionless softening law,

$$\frac{\sigma}{f_t} = f\left(\frac{w}{w_f}\right) \tag{33}$$

one obtains the integral equation

$$\int_0^{\rho} \frac{q(\omega)\mathrm{d}\omega}{\sqrt{\rho - \omega}} = F(\rho) \tag{34}$$

in which the right-hand side is

$$F(\rho) = S(1) f\left(\frac{1}{W(0)} \int_{\rho}^{1} \sqrt{\omega - \rho}\, q(\omega)\, \mathrm{d}\omega\right) \tag{35}$$

Since all the variables are dimensionless, the q-profile is independent of any dimensional parameters and depends only on the shape of the softening law. Note that the structure size D is absent from (34).

Equation (34) has a weakly singular kernel and represents an integral equation of the first kind for function $q(\rho)$. This equation, whose equivalent form in terms of $p(\rho)$ was introduced by Planas and Elices (1992) (see also Bažant and Planas (1998, Equation 7.5.67), represents the well-known Abel's integral equation if the right-hand side $F(\rho)$ is known. In the special case of a linear (triangular) softening curve ($w_f = w_0$), Equation (34) simplifies to the following linear integral equation of the first kind:

$$\frac{S(\rho)}{S(1)} + \frac{W(\rho)}{W(0)} = 1 \tag{36}$$

Getting an analytical solution of (34) is not easy. It is known only for the Dugdale-type (rectangular) softening law (Planas and Elices, 1993). The basic idea of the numerical algorithm which was invented by Planas and Elices (1993) is adapted for this study. They used a piece-wise linear approximation on uniformly spaced intervals. The uniform spacing worked well for the simple triangular softening law even with small number of subdivisions since for that law the slope of $q(\alpha)$ is quite uniform through the entire softening range.

However, for the softening laws in use for concrete, particularly bilinear softening laws with extra long tail (ELT), $q(\alpha)$ changes rapidly in the initial part. Unless a uniform mesh with very fine subdivisions is used, the error in the initial part is relatively large compared to that in the remaining part. The initial part is very important regarding the size effects for positive geometries (cases 1 and 2), and so it is advisable to use in that part a finer mesh.

Computations show that the laws characterized by a steep initial drop and a very flat long tail are reproduced from the q-profile without any noticeable error when 100 subdivisions are used. However, 100 subdivisions are not necessary. It is more efficient, and sufficient for accuracy, to refine the subdivisions only in the initial part (Figure 2). Therefore the length of the intervals in the subdivision is changed gradually from 0.01 to 0.2. This reduces the total number of subdivisions to 30 and is achieved by setting

$$\Delta\rho_i = \rho_{i+1} - \rho_i = ce^{-k\rho_i} (1 \leq i \leq 30) \tag{37}$$

in which $\rho_1 = 0.0$, $\rho_{30} = 1.0$, $c = 0.2$, and $k = 2.9458900$.

The stress and the crack opening displacement are interpolated by a set of discrete interpolation functions in which a linear shape function, $\phi(\omega)$, is used for the sake of simplicity (Figure 3);

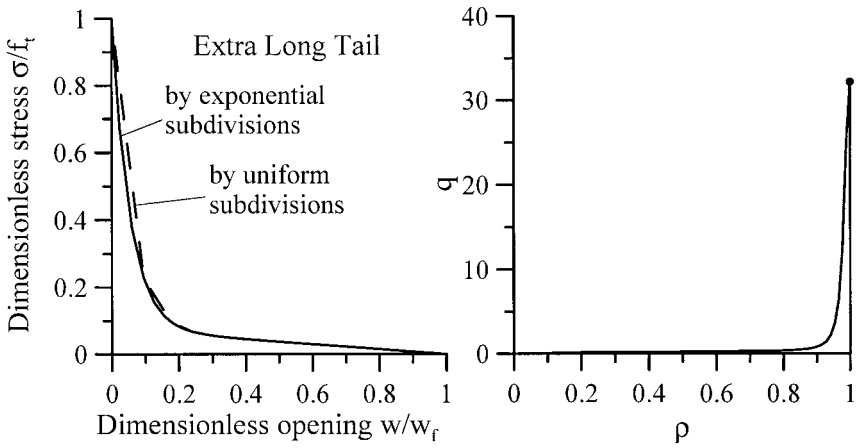

Figure 2. The softening curve (left) and the corresponding q-profile (right) reproduced with 30 subdivisions: the dashed line by uniform spacing and the solid line by exponential spacing (the latter almost coincides with the analytical curve).

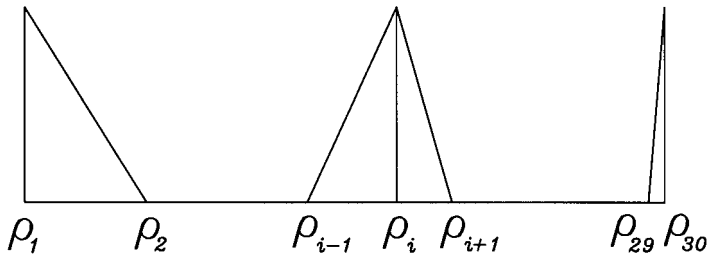

Figure 3. The linear base function with variable nodal spacing, used to approximate q-profile.

$$S(\rho_i) = \left(\int_0^{\rho_i} \frac{\phi_j(\omega)}{\sqrt{\rho_i - \omega}} \mathrm{d}\omega \right) q_j = \sum_j L_{ij} q_j \tag{38}$$

$$W(\rho_i) = \left(\int_{\rho_i}^1 \sqrt{\omega - \rho_i} \phi_j(\omega) \mathrm{d}\omega \right) q_j = \sum_j U_{ij} q_j \tag{39}$$

in which

$$\phi_j(\omega) = \begin{cases} 1 + c^{-1} e^{k\omega_{i-1}} (\omega - \omega_j) & \text{for} \quad \omega_{j-1} < \omega < \omega_j \\ 1 - c^{-1} e^{k\omega_i} (\omega - \omega_j) & \text{for} \quad \omega_j < \omega < \omega_{j+1} \\ 0 & \text{otherwise} \end{cases} \tag{40}$$

L_{ij} and U_{ij} are constant lower and upper triangular matrices, and q_j is a column matrix of nodal values. The integrals in (38) and (39) can be calculated analytically. The integral equation (34) is discretized as

$$\sum_j L_{ij} q_j = \sum_k L_{30k} q_k f \left(\frac{\sum_l U_{il} q_l}{\sum_m U_{1m} q_m} \right) \tag{41}$$

Equation (34) and its discrete form, Equation (41), are insufficient to solve the problem. There are infinitely many q-profiles as the solutions. The additional condition required to obtain a

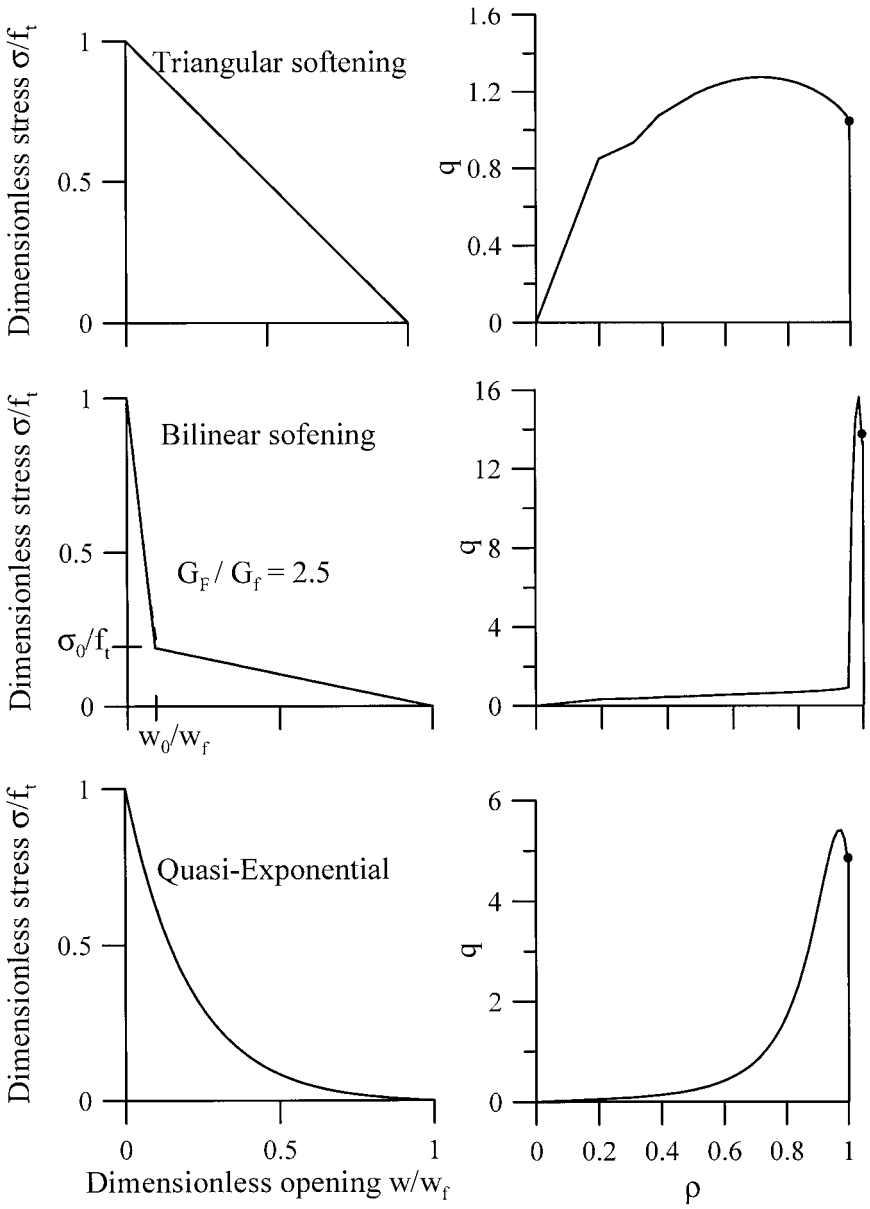

Figure 4. Analytical softening laws (solid lines) and the lines (dashed) reproduced from the q-profiles on the right using 30 exponentially varying subdivisions (the dashed lines are mostly undistinguishable from the solid input lines).

unique q-profile is Equation (10) stating that the area under the q-profile must be 1.0. Practically, it is preferable to solve Equation (41) first for a fixed value of one of q_i, typically q_{30}, and subsequently scale the q-profile to make the area equal to 1.0, according to Equation (10). An iterative algorithm to compute the q-profile may be summarized as follows: (a) Compute the right hand-side of Equation (41) using the previous iterate of the q-profile, but for the first iteration assume a uniform q-profile. (b) Solve the q-profile from the left hand side of

Table 1. The stress intensity factor density profiles for triangular, bilinear, and ELT softening laws.

ρ	Triangular	Petersson (1981)	Wittmann et al. (1988)			Exponential	
			(0.157,0.250)	(0.135,0.250)	(0.111,0.250)	QEX	ELT
0.000000	0.000000	0.000000	0.000000	0.000000	0.000000	0.000000	0.000000
0.200000	0.849558	0.407870	0.345225	0.359922	0.380037	0.051842	0.155200
0.310957	0.935248	0.453959	0.383966	0.400044	0.422105	0.087204	0.172577
0.390976	1.075710	0.534354	0.452865	0.471300	0.496616	0.132242	0.205593
0.454192	1.138059	0.578381	0.490984	0.510397	0.537094	0.183185	0.224934
0.506666	1.189093	0.618765	0.526186	0.546361	0.574146	0.243189	0.243451
0.551624	1.221442	0.650946	0.554434	0.575017	0.603419	0.313197	0.259082
0.591005	1.244511	0.679408	0.579501	0.600299	0.629063	0.394961	0.273567
0.626073	1.259665	0.704663	0.601756	0.622591	0.651492	0.490180	0.287083
0.657699	1.269262	0.727873	0.622132	0.642860	0.671722	0.600815	0.300132
0.686511	1.274452	0.749667	0.641084	0.661574	0.690243	0.728994	0.313050
0.712979	1.276206	0.770678	0.659045	0.679170	0.707505	0.877034	0.326239
0.737462	1.275186	0.791498	0.676349	0.695976	0.723842	1.014386	0.340168
0.760241	1.271902	0.812841	0.693303	0.712288	0.739543	1.242564	0.355454
0.781541	1.266734	0.835807	0.710201	0.728373	0.754866	1.465014	0.372955
0.801546	1.259980	0.935720	0.727356	0.744503	0.770056	1.716919	0.393914
0.820406	1.251865	2.144074	0.745135	0.760971	0.785366	1.999901	0.420192
0.838247	1.242566	2.418016	0.764013	0.778127	0.801078	2.314625	0.454650
0.855175	1.232218	2.802637	0.784688	0.796426	0.817530	2.660252	0.501808
0.871279	1.220921	3.034241	0.808358	0.816527	0.835166	3.033773	0.569015
0.886636	1.208748	3.225127	0.837889	0.839519	0.854622	3.429217	0.668607
0.901315	1.195744	3.354861	2.777613	0.867696	0.846912	3.836824	0.822097
0.915372	1.181927	3.440242	4.506939	1.669777	0.903931	4.242291	1.068711
0.928859	1.167286	3.483223	5.373447	5.204020	0.940655	4.626306	1.483876
0.941821	1.151773	3.488585	6.055927	6.166555	5.037750	4.964558	2.221969
0.954297	1.135289	3.458570	6.434490	7.199171	7.466705	5.228402	3.621996
0.966323	1.117649	3.394475	6.587814	7.624333	8.769636	5.385983	6.479251
0.977930	1.098500	3.295290	6.510574	7.710255	9.322868	5.402767	12.660595
0.989147	1.077056	3.155056	6.200630	7.380761	9.089455	5.236620	24.942680
1.000000	1.050158	2.941343	5.551491	6.520243	7.902657	4.777411	32.044469
I_1	1.000000	1.000000	1.000000	1.000000	1.000000	1.000000	1.000000
I_2	0.577231	0.740843	0.786831	0.784721	0.779617	0.849376	0.895147
I_3	1.489370	1.268471	1.223341	1.228947	1.237885	1.109404	1.105492
I_4	0.737093	0.844129	0.871412	0.869547	0.865837	0.916790	0.937519
I_5	1.223914	1.599210	1.715875	1.713136	1.703099	1.843406	1.983880
$S(1)$	2.148285	3.361051	4.437308	4.710724	5.040733	4.283968	9.622699
$W(0)$	0.737064	0.844131	0.871414	0.869549	0.865837	0.916787	0.937518

Table 2. The stress intensity factor density profiles for bilinear softening curves, whose $G_F/G_f = 2.5$.

ρ	The positions of the kink points $(\bar{\omega}, \bar{\sigma})$					
	(0.077, 0.150)	(0.091, 0.190)	(0.102,0.230)	(0.111,0.270)	(0.118,0.310)	(0.123,0.350)
0.000000	0.000000	0.000000	0.000000	0.000000	0.000000	0.000000
0.200000	0.316602	0.343269	0.370938	0.398944	0.427620	0.432327
0.310957	0.351732	0.381310	0.411978	0.442992	0.474715	0.479922
0.390976	0.415006	0.449346	0.484862	0.520692	0.557240	0.563235
0.454192	0.450013	0.486690	0.524536	0.562623	0.601369	0.607719
0.506666	0.482397	0.521082	0.560898	0.600868	0.641414	0.648055
0.551624	0.508379	0.548492	0.589674	0.630910	0.672621	0.679448
0.591005	0.531410	0.572666	0.614914	0.657109	0.699667	0.706628
0.626073	0.551804	0.593957	0.637016	0.679910	0.723046	0.730098
0.657699	0.570396	0.613276	0.656967	0.700381	0.743911	0.751024
0.686511	0.587581	0.631056	0.675243	0.719039	0.762819	0.769972
0.712979	0.603727	0.647699	0.692280	0.736355	0.780283	0.787461
0.737462	0.619103	0.663499	0.708399	0.752681	0.796682	0.803874
0.760241	0.633942	0.678710	0.723878	0.768319	0.812345	0.819546
0.781541	0.648446	0.693555	0.738961	0.783536	0.827565	0.834777
0.801546	0.662803	0.708241	0.753878	0.798588	0.842627	0.849856
0.820406	0.677200	0.722977	0.768861	0.813737	0.857830	0.865092
0.838247	0.691834	0.737983	0.784164	0.829276	0.873516	0.880841
0.855175	0.706924	0.753514	0.800081	0.845557	0.890120	0.897561
0.871279	0.722734	0.769878	0.816985	0.863048	0.908254	0.915911
0.886636	0.739599	0.787481	0.835385	0.882426	0.928898	0.936985
0.901315	0.757974	0.806895	0.856038	0.904794	0.953994	0.963170
0.915372	0.778518	0.828992	0.880197	0.932329	1.296577	1.889660
0.928859	0.802268	0.855254	0.910307	1.160857	4.602187	4.553272
0.941821	0.831040	0.888635	0.953199	5.943449	5.383692	5.331318
0.954297	0.868585	0.937576	7.678646	7.005794	6.302668	6.116189
0.966323	0.926129	10.102043	9.662315	8.197928	6.667001	6.436074
0.977930	15.104265	14.495522	11.102572	8.492573	6.746275	6.485222
0.989147	24.265599	15.633470	11.012774	8.251976	6.463856	6.208868
1.000000	20.541118	13.296150	9.477575	7.187407	5.714078	5.501976
I_1	1.000000	1.000000	1.000000	1.000000	1.000000	1.000000
I_2	0.818640	0.802502	0.786210	0.770147	0.754319	0.751668
I_3	1.197232	1.214172	1.231511	1.248835	1.266240	1.269128
I_4	0.889308	0.879580	0.869715	0.859947	0.850261	0.848643
I_5	1.801305	1.760774	1.720067	1.680131	1.641060	1.634497
$S(1)$	7.771279	6.369514	5.455790	4.809113	4.330614	3.966973
$W(0)$	0.889307	0.879579	0.869715	0.859946	0.850261	0.840629

Equation 41). (c) Scale the q-profile according to the unit area condition of Equation (10). (d) Go to (a) and repeat the entire procedure unless a prescribed tolerance has been met.

The softening laws reproduced from the q-profiles for the assumed triangular, bilinear and quasi-exponential softening stress-displacement laws are compared in Figure 4. The differences are in most places invisible.

The q-profiles for the triangular, Petersson's (1981), Wittmann et al.'s (1988) and exponential softening laws are tabulated in Table 1. In addition to that, Table 2 gives the q-profiles for various bilinear softening laws that have different locations of the 'kink' (or knee) point (point of slope change) but are characterized by the same ratio of the total area to the area under the initial segment, $G_F/G_f = 2.5$. The ratio of 2.5 is a rough mean estimate for concrete, made by Planas et al. (1992), (Guinea et al., 1994), and was found to agree optimally with extensive test data by Bažant and Becq-Giraudon (2001). The q-profiles for bilinear softening stress-displacement laws with other locations $(\bar{w}, \bar{\sigma}) \equiv (w_0/w_f, \sigma_0/f_t)$ of the 'kink' points, can be obtained by interpolation from Table 2.

It is interesting to see how q-profiles are related to the size effect law. When $q = 1.0$, one gets Equation (23) corresponding to the classical Bažant's size effect law (Bažant, 1984). The effective fracture process zone length c_f obtained by fitting this classical size effect law to the test data is about 30% greater than one half of the length of the actual cohesive zone l_f because $I_2 \approx 0.75$ (see the tables attached).

4. Conclusions

1. The smeared-tip method characterized by the profile of the stress intensity factor density is an effective approach to solving cohesive crack problem, suited particularly for large-size asymptotic approximations. In this method, the large-size asymptotic profile of the stress intensity factor density (q-profile) can be regarded as a material characteristic that is uniquely related to the softening stress-displacement law of the cohesive crack.
2. An efficient and accurate algorithm for computing the asymptotic q-profile for a given softening stress-displacement law of cohesive crack is developed. It is based on solving a singular Abel's integral equation. Tables giving the q-profiles for various typical softening laws are presented. The q-profiles for various bilinear softening laws can be obtained by interpolation from the table.
3. If the q-profiles of a given softening stress-displacement law and the function giving the stress intensity factor as a function of the crack length are known, one can obtain the solutions of cohesive fracture problems without solving the integral equation of the cohesive crack model and without resorting to finite element analysis.
4. The present solution can be expected to be accurate only if the fracture process zone does not end with a significant stress jump. This is the case for maximum loads of structures of initially negative geometry (K_I decreasing with crack length). For positive geometry, this limits applicability to large enough structures.

Acknowledgements

Partial financial support under grant CMS-9732791 from National Science Foundation to Northwestern University and grant DE-FG07-98ER45736 from the Department of Energy is gratefully acknowledged.

References

Barenblatt, G. I. (1959). The formation of equilibrium cracks during brittle fracture, general ideas and hypothesis, axially symmetric cracks. *Prikladnaya Matematika i Mekhanika* **23**(3), 434–444.

Barenblatt, G. I. (1962). The mathematical theory of equilibrium of cracks in brittle fracture. *Advances in Applied Mechanics* **7**, 55–129.

Bažant, Z. P. (1983). Fracture in concrete and reinforced concrete. Preprints, IUTAM Prager Symposium on *Mechanics of Geomaterials: Rocks, Concretes, Soil*, (edited by Z. P. Bažant, Northwestern University, Evanston, 281–316.

Bažant, Z. P. (1984). Size effect in blunt fracture: Concrete, rock, metal. *Journal of Engineering Mechanics, ASCE* **110**, 518–535.

Bažant, Z. P. (1990). Smeared-tip superposition method for nonlinear and time-dependent fracture. *Mechanics Research Communications* **17**(5), 343–351.

Bažant, Z. P. (2001). Size effects in quasibrittle fracture: Apercu of recent results. *Fracture Mechanics of Concrete Structures* (Proc., FraMCoS-4 Int. Conf., Paris), R. de Borst, J. Mazars, G. Pijaudier-Cabot and J.G.M. van Mier (eds.), Swets & Zeitlinger (A.A. Balkema Publishers), Lisse, 651–658.

Bažant, Z. P. (2002). *Scaling of Structural Strength*, Hermes-Penton Science, London.

Bažant, Z. P. and Becq-Giraudon, E. (2001). Statistical prediction of fracture parameters of concrete and comparison of testing methods. *Cement and Concrete Research* **32**(4), 529–556.

Bažant, Z. P. and Beissel, S. (1994). Smeared-tip superposition method for cohesive fracture with rate effect and creep. *International Journal of Fracture* **65**, 277–290.

Bažant, Z. P. and Li, Y.-N. (1995). Stability of cohesive crack model: Part II—Eigenvalue analysis of size effect on strength and ductility of structures. Trans. ASME, *Journal of Applied Mechanics* **62**, 965–969.

Bažant, Z. P. and Planas, J. (1998). *Fracture and Size Effect in Concrete and Other Quasibrittle Materials*, CRC Press, New York.

Guinea, G. V., Planas, J. and Elices, M. (1994). Correlation between the softening and the size effect curves. *Size Effect in Concrete Structures*, H. Mihashi, H. Okamura and Z. P. Bažant, eds., E&FN Spon, London, 233–244.

Hillerborg, A., Modéer, M. and Petersson, P.E. (1976). Analysis of crack formation and crack growth in concrete by means of fracture mechanics and finite elements. *Cement and Concrete Research* **6**, 773–782.

Kfouri, A. P. and Rice, J.R. (1977). Elastic-plastic separation energy rate for crack advance in finite growth steps, *Fracture 1977*, (Proc. 4th Int. Conf. on Fracture, ICF4, Waterloo), D. M. R. Taplin, ed., Univ. of Waterloo, Ontario, Canada, Vol. 1, 43–59.

Knauss, W. G. (1973). The mechanics of polymer fracture, *Appled Mechanics Reviews* **26**, 1–17.

Knauss, W. G. (1974). On the steady propagation of a crack in a viscoelastic sheet: Experiments and analysis, *Mechanics of Fracture*, F. Erdogan, ed., ASME, New York, (AMD-19), 69–103.

Murakami, Y. (1986). *Stress intensity factors handbook*, 1st edition, Pergamon, Oxford.

Needleman, A. (1990). An analysis of tensile decohesion along an interface. *Journal of the Mechanics and Physics of Solids* **38**(3), 289–324.

Palmer, A. C. and Rice, J.R. (1973). The growth of slip surfaces on the progressive failure of over-consolidated clay. *Proceedings of The Royal Society of London, Series A*. **332**, 527–548.

Petersson, P. E. (1981). *Crack growth and development of fracture zone in plain concrete and similar materials*, Report No. TVBM-1006, Division of Building Materials, Lund Institute of Technology, Lund, Sweden.

Planas, J. (1986). Un nuevo método de análisis del comportamiento de una fisura cohesiva en Modo I. *Anales de Mecánica de la Fractura* **3**, 219–227.

Planas, J. and Elices, M. (1992). Asymptotic analysis of a cohesive crack: 1. Theoretical background. *International Journal of Fracture* **55**, 153–177.

Planas, J. and Elices, M. (1993). Asymptotic analysis of a cohesive crack: 2. Influence of the softening curve. *International Journal of Fracture* **64**, 221–237.

Planas, J., Elices, M. and Guinea, G.V. (1992). Measurement of the fracture energy using three-point bend tests: Part 2—Influence of bulk energy dissipation. *Materials and Structures* **25**, 305–312.

Planas, J., Elices, M. and Guinea, G.V. (1994). Cohesive cracks as a solution of a class of nonlocal models, in *Fracture and Damage of Quasibrittle Structures*, Z. P. Bažant, Z. Bittnar, M. Jirásek and J. Mazars, eds., E & FN Spon, London, 131–144.

Rice, J. R. (1968). Path independent integral and approximate analysis of strain concentrations by notches and cracks. *Journal of Applied Mechanics, ASME* **35**, 379–386.

Smith, E. (1995). Recent research on the cohesive zone description of an elastic softening material, in *Fracture of Brittle Disordered Materials: Concrete, Rock, Ceramics*, G. Baker and B. L. Karihaloo, eds., E & FN Spon, London, 450–463.

Smith, E. (1999). The effect of the stress-relative displacement law on failure prediction using the cohesive crack model. *International Journal of Fracture* **91**, 41–51.

Tada, H., Paris, P.C. and Irwin, G.R. (1985). *The stress analysis of cracks handbook*, Del Research Corp., Hellertown, PA..

Wittmann, F. H., Rokugo, K., Brühwiler, E., Mihashi, H. and Simonin, P. (1988). Fracture energy and strain softening of concrete as determined by means of compact tension specimens. *Materials and Structures* **21**, 21–32.

Zi, G. and Bažant, Z.P. (2002). Eigenvalue method for computing size effect of cohesive crack with residual stress, with application to kink bands in composites. *International Journal of Engineering Science*, in press.